The structure of Rph, an exoribonuclease from *Bacillus anthraci* ° resolution.

<-Hidden text (press ¶ or see Help)

Andrea E. Rawlings, Elena V. Blagova, Vladimir M. Levdikov, Mark J. Fogg, Keith S. Wilson and Anthony J. Wilkinson*

York Structural Biology Laboratory, Department of Chemistry, The University of York, York, YO10 5YW, UK. E-mail: ajw@ysbl.york.ac.uk

Synopsis The crystal structure of a phosphate dependent exoribonuclease from *Bacillus anthracis*, has been solved to 1.7 Å resolution. The refined model reveals a hexameric ring structure and five bound sulphate ions per subunit. Each subunit features two sulphate ions located in the active site.

Abstract Maturation of tRNA precursors into functional tRNA molecules requires trimming of the primary transcript at both the 5' and 3' ends. Cleavage of nucleotides from the 3' stem of tRNA precursors, releasing nucleotide diphosphates, is accomplished in *Bacillus* by a phosphate dependent exoribonuclease, Rph. The crystal structure of this enzyme from *Bacillus anthracis* has been solved by molecular replacement to a resolution of 1.7 Å and refined to an *R* factor of 19.3%. There is one molecule in the asymmetric unit; the crystal packing reveals the assembly of the protein into a hexamer arranged as a trimer of dimers. The structure shows two sulphate ions bound in the active site pocket, probably mimicking the phosphate substrate and the phosphate of the 3' terminal nucleotide of the tRNA precursor. Three other bound sulphate ions point to likely RNA binding sites.

Keywords: Exoribonuclease; *Bacillus anthracis*; tRNA maturation; crystal structure; RNase Ph.

1. Introduction

Transfer RNA molecules are transcribed as precursors with additional nucleotides on both their 5' and 3' ends. These flanking sequences must be cleaved off to reveal the mature, functional tRNA species. In *Bacillus,* as in most organisms, endonucleolytic cleavage of the 5' extension is performed by RNase P, a hetero-tetrameric ribonucleoprotein complex (Stams *et al.*, 1998, Fang *et al.*, 2001). However, the manner in which the 3' nucleotides are removed varies from species to species. In *Escherichia coli*, the most studied system, the 3' flanking sequence is first trimmed by an endoribonuclease such as RNase E and this is followed by exoribonucleolytic degradation by one or more of a number of enzymes including RNase II, RNase BN, RNase T and RNase Ph. In *Bacillus* just two enzymes are known to process the 3' termini, an endoribonuclease called RNase Z, and the exoribonuclease RNase Ph, (Pellegrini *et al.*, 2003, Wen *et al.*, 2005).

RNase PH is a member of the phosphate dependent 3' → 5' exoribonuclease (PDX) family (Zuo & Deutscher, 2001, Mian, 1997). This family includes polynucleotide phosphorylase, PNPase, and a shared characteristic is the

utilisation of inorganic orthophosphate in the cleavage reactions (Deutscher *et al.*, 1988), to generate nucleoside diphosphates, rather than the more common nucleoside monophosphates formed by the hydrolytic ribonucleases.

Bacillus anthracis, the causative agent of anthrax, is a soil-dwelling, Gram positive endospore-forming bacterium. Its genome has been sequenced (Read *et al.*, 2003), revealing the presence of an open reading frame that shares a high degree of identity with the well-characterised RNases PH from *Bacillus subtilis, E.coli* and other bacteria. Here we report the determination of the structure of Rph from *B. anthracis Ames*, a target in a high throughput structural genomics study.

2. Materials and methods

2.1. Cloning, expression and purification

The *rph* coding sequence was amplified by PCR from *B. anthracis Ames* genomic DNA using BA4715F (5'-CACCACCACCACATGCGAGTAGATGGTAGAGAGAAAA-3') as a forward primer and BA4715R (5'-GAGGAGAAGGCGCGTTACTACTCTATATGAGATACGATGTCACCTAAC-3') as a reverse primer and cloned using a ligation independent cloning method (Alzari *et al.*, 2006, Au *et al.*, 2006, Fogg & Wilkinson, 2008). The resulting fragment was treated with T4 DNA polymerase in the presence of dATP to generate single stranded DNA overhangs complementary to those present on a modified pET28a vector cut with BseR1 and then similarly treated with T4 DNA polymerase in the presence of dTTP. The vector and PCR products were incubated together for 20 minutes to allow annealing of the single-stranded overhang regions (Aslanidis & de Jong, 1990), and the mixture was added directly to *E. coli* Novablue competent cells (Novagen) which were plated and grown overnight on antibiotic-containing media. Kanamycin-resistant colonies were picked the following day and used to inoculate overnight cultures from which recombinant plasmids were purified. The resulting plasmid pETBaRph contains the coding sequence of *rph* fused to the coding sequence for an N-terminal MGSSHHHHHH tag. pETBaRph was introduced into *E. coli* BL21 (DE3) for overproduction of recombinant Rph.

N-terminally hexa-histidine tagged Rph was expressed from *E. coli* BL21 (DE3)/pETBaRph by overnight growth in kanamycin supplemented autoinduction media (Studier, 2005) at 310 K. Cells from 0.5 l of culture were harvested by centrifugation at 5000 rpm for 15 minutes. Pelletted cells were resuspended in buffer A (20 mM Na_2HPO_4, 0.5 M NaCl, 10 mM imidazole pH 7.5) and lysed by sonication. Further centrifugation at 15000 rpm generated a cleared lysate which was loaded onto a 5 ml HiTrap^{TM} nickel chelation column, from which Rph was eluted following the application of a linear gradient of 10 mM to 500 mM imidazole in buffer A. Peak fractions were automatically directed on to a HiLoad 16/60 Superdex 200 prep-grade gel-filtration column (GE Healthcare) previously equilibrated with buffer B (50 mM Tris-HCl pH 7.5, 150 mM NaCl). The protein eluted with high purity and by comparison with the elution profiles of standard proteins the oligomerisation state of Rph was determined to be

hexameric. The 37.6 mg of purified protein obtained were concentrated to 20 mg ml^{-1} in Buffer B, aliquoted and stored at 193 K.

2.2. Crystallization

A Mosquito nanolitre pipetting robot was used for screening Rph against different crystallization conditions using sitting drop vapour diffusion in a 96-well plate format. 150 nl drops were equilibrated against 80 µl of reservoir solution at 293 K. Small crystals were obtained in the Clear strategy screen (Brzozowski & Walton, 2001) with a reservoir solution comprising 2.7 M ammonium sulphate and 0.1 M Bis-Tris pH 5.5. These conditions were altered systematically, including a change to hanging drop vapour diffusion in 24-well plates to optimise the crystal quality. Large, single crystals appeared in 2 µl drops made up from 1 µl of 2 M ammonium sulphate and 0.2 M K/Na tartrate, and 1 µl of protein at a concentration of 20 mg ml^{-1}.

2.3. Data collection and processing

A single crystal was mounted in a cryo-loop (Hampton) and flash cooled in liquid nitrogen following a brief immersion in a cryoprotectant composed of reservoir solution supplemented with 30 % (v/v) glycerol.

Diffraction data were collected on beamline ID14.3 at the European Synchrotron Radiation Facility (ESRF). The crystal was maintained at a constant 100 K throughout the experiment and exposed to radiation of wavelength 0.931 Å. Images were collected on an ADS Q4R detector. Indexing of the diffraction patterns with *DENZO* from the HKL2000 program suite (Otwinowski *et al.*, 1997) showed the crystal belonged to the space group R32, with unit cell parameters of $a = b = 86.87$ Å, $c = 179.31$ Å. The diffraction images revealed that the low resolution spots were surrounded by regions of diffuse scattering, due to semi-ordered water-ice structure. Integration and scaling of the data were performed using *XDS* (Kabsch, 1988) and *SCALA* respectively (CCP4, 1994). The data statistics are presented in Table 1.

2.4. Structure solution and refinement

MOLREP (Vagin & Teplyakov, 1997, Murshudov *et al.*, 1997) was used to solve the structure by molecular replacement using a single subunit of the RNase PH structure (PDB code 1OYR) from *B. subtilis* (which shares 69 % sequence identity with Rph) (Harlow *et al.*, 2004) as the search model. After performing rotation and translation functions a clear solution was found with an initial R factor of 49.1%, compared to the next best solution with an R factor 63.4%. The solution shows a single molecule in the asymmetric unit indicating a solvent content of 48.8 %. Rigid body and TLS refinement were performed using REFMAC (Murshudov *et al.*, 1997). At the stage, changes in sequence between the *B. subtilis* Rph search model and the B. anthracis Rph structure were apparent in the electron density maps (Fig. 1). Structure refinement continued with successive rounds of model building in COOT (Emsley & Cowtan, 2004) followed by REFMAC refinement. The final R-factor for the structure consisting of 2090 atoms and

168 water molecules is 19.26 % (R_{free} = 24.07 %). Protein structure and ligand analysis was performed using the pdbsum server (Laskowski, 2001).

Table 1 X-ray data and refinement statistics.

Data Collection	
Space Group	R32
Unit cell parameters (Å, ^{O})	a = 86.75, b= 86.75, c = 179.08
	α = 90.0, β = 90.0, γ = 120.0
Resolution range (Å)	43.36-1.70
No. unique reflections	28380
Completeness (%) †	98.7 (95.6)
Redundancy †	7.3 (5.7)
R_{merge} [a†]	0.040 (0.38)
I/σ(I) †	25.2 (4.8)
Refinement	
Resolution range (Å)	35.09 - 1.70
R factor[b]	0.193
R_{free} [c]	0.241
No. subunits in asym. unit	1
No. protein non-H atoms	1901
No water molecules	168
No. sulphates	5
No. TLS groups	6
B factors (Å^2) average	
Solvent	11.2
Main chain	7.9
Side chain	10.3
R.m.s.d bond lengths[d] (Å)	0.022
R.m.s.d bond angles[d]	1.980
Ramachandran plot	
Most favoured (%)	92.6
Additionally allowed (%)	7.4

† Data for the highest resolution shell 1.79 -1.70 is shown in brackets

[a] $R_{merge} = \sum_{hkl}\sum_i (I_i - \langle I \rangle) / \sum_{hkl}\sum_i \langle I \rangle$ where I_i is the intensity of the *i*th measurement of a reflection with indexes *hkl* and $\langle I \rangle$ is the statistically weighted average reflection intensity.

[b] *R*-factor = $\sum (F_O - F_C) / \Sigma F_O$ where F_O and F_C are the observed and calculated structure factor amplitudes, respectively.

[c] *R*-free is the *R*-factor calculated with 5 % of the reflections chosen at random and omitted from refinement.

[d] Root-mean-square deviation of bond lengths and bond angles from ideal geometry.

3. Results and Discussion

The structure of Rph from *B. anthracis* was solved to 1.7 Å resolution, with a single protein molecule in the asymmetric unit. The protein chain assumes the βαβα topology (Fig 2a), seen in other RNase Ph structures (Harlow *et al.*, 2004), consisting of nine β-strands and five α-helices. It can be thought of as a double-sandwich with strands 1-5 and 6-9 surrounding helices 1-3, and helices 1-3 and 4-5 surrounding strands 6-9. Analysis of the molecular packing revealed that Rph is a hexamer (Fig. 2b) arranged as a trimer of dimers as indicated by the crystal symmetry. The β9 strands from a pair of subunits come together so that an 8 stranded inter-subunit β-sheet is formed featuring strands 6-9 from the two adjacent subunits. The dimer has a buried surface area of 1523 $Å^2$; 10 % of which is accounted for by Arg212 present on strand β9 that also makes 4 hydrogen bonds across the interface. The trimer is formed predominantly through contacts between the loops linking strands 1-5 with 1465 $Å^2$ buried at this surface. His23, Arg68, Arg76, Arg73, Asp115 and 117 and Gln120 all of which are conserved residues, collectively contribute over 40 % to this surface area and 70 % of the hydrogen bond interactions.

The loop region between strand β5 and helix α2, which is found in the centre of the hexamer, is poorly defined in the electron density maps and as a result the lysine at position 80 is omitted from the refined model. It has been suggested that this loop, with its arginine rich character is prone to proteolytic degradation, and that the hexamer may be a storage mechanism to protect the loops (Harlow *et al.*, 2004).

Rph from *B. anthracis* shares a high degree of sequence similarity with its orthologues from *B. subtilis* and *E.coli*, 69 % and 56 % identity respectively (Fig. 3). The five sulphate ions bound to the *B. anthriacis* Rph (Table 2, Fig. 2a, Fig. 4) make contacts with residues that are conserved, possibly indicating a role as tRNA phosphate mimics, with two located in the active site pocket (Fig. 5). The first sulphate (Sul1), a likely mimic of the phosphate substrate, makes contacts with the highly conserved residues Arg86, Gly124, Thr125 and Arg126 (situated on helices 1 and 3), which have been shown to play important roles in the phosphorolytic reaction. This sulphate is located in a position equivalent to that of the bound tungstate in PNPase from *Streptomyces antibioticus* (Symmons *et al.*, 2000), the phosphate bound in the structure of Rph from *Aquifex aeolicus* (Ishii *et al.*, 2003), and the sulphate found in the active site of RNase PH from *B. subtilis* (Harlow *et al.*, 2004). The second sulphate ion (Sul2) is bound to residues Arg86 and Arg126, as well as Arg92 from the neighbouring dimer forming subunit. It is probable that this sulphate mimics the phosphate of the 3' terminal phosphodiester bond found on the tRNA substrate. The presence of Sul2 in the active site may help to order the Arg 86 side-chain, which was poorly defined in the *B. subtilis* structure that featured just a single sulphate ion. The sulphur atoms of Sul1 and Sul2 are 6.3 Å apart (Fig. 5). It appears that Arg86 and Arg126, that have contacts with both sulphates, ensure that the substrate tRNA and the phosphate nucleophile assume the appropriate juxtaposition within the active site. Attack of the phosphate's nucleophilic oxygen at the phosphorus centre of the 3' terminal nucleotide, thought to progress by an S_N2 type mechanism, would result in the

transient formation of a penta-coordinate phosphorus species (Mildvan, 1997). The conserved arginine residues in the active site may help to stabilise this negatively charged transition state.

The third sulphate ion (Sul3), which is in contact with Arg99 has also been observed in the structure of RNase PH from *B. subtilis* and from *Aquifex aeolicus* where additional interactions with Trp 58 and Thr 60 are made (Harlow *et al.*, 2004, Ishii *et al.*, 2003). It is possible that the dimerisation of two Rph subunits allows insertion of the 3' terminus of the tRNA precursor into the active site pocket of molecule 1 with phosphates present elsewhere in the substrate interacting with residues 99, 58 and 60 of molecule 2. Sulphate 4 is hydrogen bonded to Arg 73, a conserved residue from the motif RX_4RX_2R beginning at residue 68, and located at the trimer interface. A fifth sulphate (Sul5) forms hydrogen bonds with Lys156, Leu104, Val102, and Lys56, and is also seen in the structure of RNase PH from *Aquifex aeolicus* (Ishii *et al.*, 2003).

The conserved N-terminal motif RX_3RX_5R beginning at Arg2 (Zuo & Deutscher, 2001), which in this structure is associated with the binding of a fifth sulphate (Sul5) at Arg 6, is unusually followed by three regularly spaced histidines at positions 13, 15, and 17. If the RX_3RX_5R sequence is involved in interactions with the RNA, as proposed for the corresponding motif in PNPase (Symmons *et al.*, 2002), then the histidines may form a base-stacking interaction with RNA bases, although these histidine residues are not strongly conserved among other members of the PDX family.

In conclusion, amongst the other RNase PH structures, the structure of Rph from *B. anthracis* is distinct in exhibiting two sulphate ligands within the active site, possibly mimicking the 3'-terminal phosphate of both the tRNA substrate and the phosphate nucleophile. Other bound sulphates indicate likely tRNA binding sites. The conserved motif $RX_5RX_3RX_2R$ beginning at Arg86 and found in helix α1 has contacts with Sul1, Sul2, Sul3, as well as Sul2 of the adjacent subunit through interaction with residue Arg92. This suggests the dimer may be the required for the catalysis.

Table 2 A list of the bound sulphate ions and interacting residues present in the *B. anthracis* Rph structure.

Sulphate Identifier	Sulphate Interaction with Rph.
Sul1	Arg86 NH2, Gly124 N, Thr125 OG1 N, Arg126 N NE NH2
Sul2	Arg86 NE, Arg126 NH2, Arg92* NH1 NH2
Sul3	Arg99 NH1
Sul4	Lys56 NZ, Leu104 N, Glu105 N, Lys156 NZ
Sul5	Arg6 NE NH2, Asn177 ND

*Arg92 is from an adjacent dimer forming subunit.

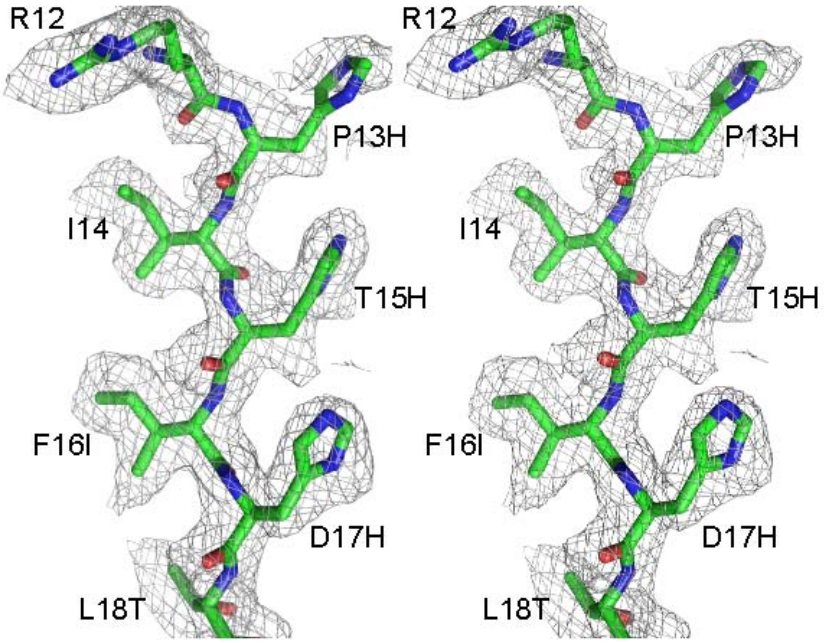

Figure 1 Stereo view of residues 12-18 of strand β1 shown in stick form and coloured by atom type. The electron density, shown in grey mesh at a contour level of 1.0 σ, is from an F_{obs}-F_{calc} omit map. The map was generated by deleting residues 12-18 from the molecular replacement model, after carrying out TLS/rigid-body-refinement. 10 cycles of REFMAC5 refinement were carried out prior to calculation of the map. This map is displayed on the final refined *B. subtilis* Rph model. Residues are labelled with the changes in sequence from the *B. subtilis* search model to the *B. anthracis* structure indicated. The stereo figure generated with PyMOL (DeLano, 2008).

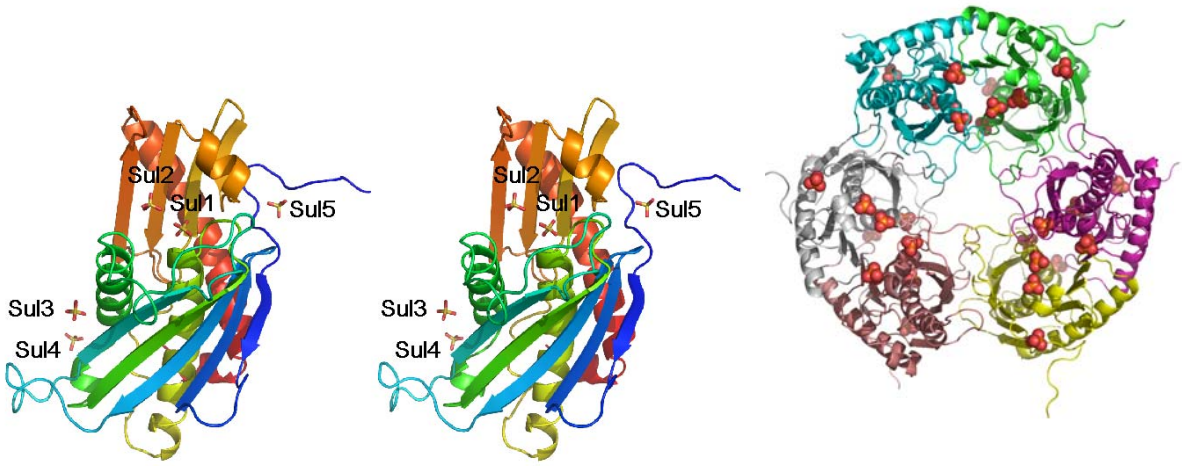

Figure 2. (a) Stereo ribbon diagram of Rph from *Bacillus anthracis* in which the chain is colour-ramped from deep blue at the N-terminus to red at the C-terminus. Bound sulphates are shown in stick format, coloured by atom type, sulphur in orange and oxygen in red. The labels correspond to those in Table 2. (b) Ribbon diagram showing the hexamer of Rph viewed along the 3-fold axis and coloured by subunit with the bound sulphates shown as spheres. Both figures generated with PyMOL (DeLano, 2008)

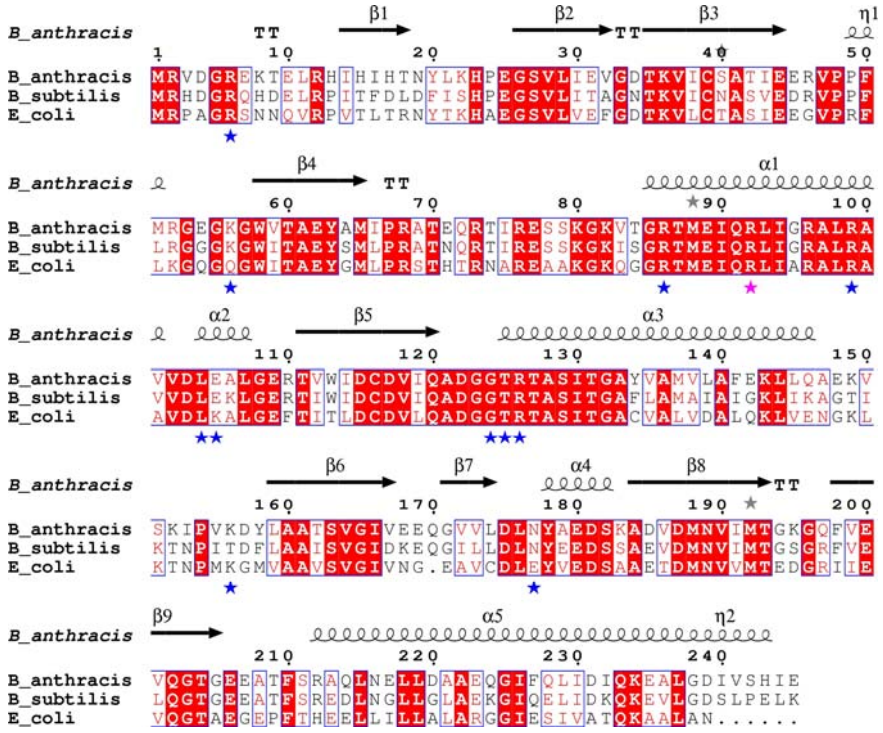

Figure 3. Sequence alignment of Rph from *B. anthracis* (Q81LA9), *B. subtilis* (P28619) and *E. coli* (P03842), using CLUSTALW (Thompson *et al.*, 1994) and formatted using ESPRIPT (Gouet *et al.*, 1999). Their UniProt accession numbers are present in parenthesis, Red boxes represent conserved residues. Blue stars show the residues that interact with the bound sulphate ions. Arg92 is highlighted with a magenta star to show that this residue makes contacts with Sul2 of the neighbouring subunit. The secondary structure elements of Rph from *B. anthracis* are depicted above the alignment. Structural elements labelled α indicate α-helix, β indicate β strands, η indicate 3_{10} helices, and TT are turns.

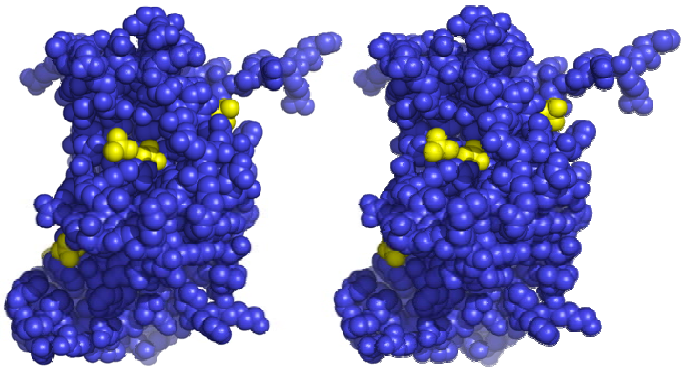

Figure 4. Stereo space filling diagram of a single subunit of Rph in blue, with bound sulphates in yellow. The Rph molecule is oriented as in Fig. 2a. Figure generated with PyMOL (DeLano, 2008).

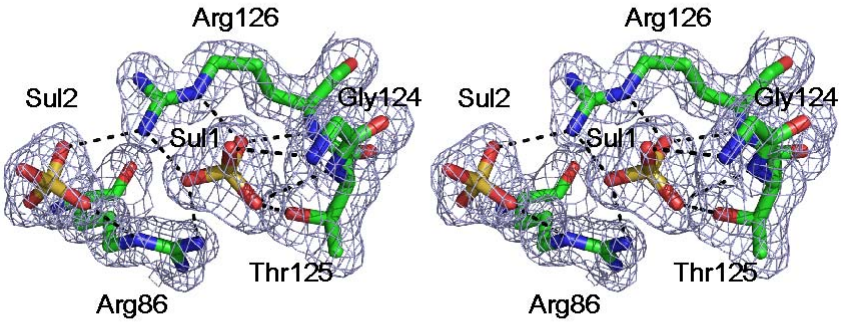

Figure 5. Stereo view of the electron density in the vicinity of the active site. Sulphates (Sul) 1 and 2 and the interacting residues, Arg86, Gly124, Thr125, and Arg126 are shown in stick form and coloured according to element. The electron density map is shown at a contour level of 1.0 σ in grey. Hydrogen bonds between the sulphates and the protein are denoted by dashed black lines. The figure generated with PyMOL (DeLano, 2008).

Acknowledgements The work described here was funded by the European Commission as SPINE contract No. QLG2-CT-2002-00988 under the RTD programme `Quality of Life and Management of Living Resources'. AER is funded by the BBSRC and VL by the Wellcome Trust. The authors would like to thank Sam Hart and Dr Tracey Gloster, of the York Structural Biology Laboratory, for their help with data collection at the ESRF, and Dr Garib Murshudov for useful advice and assistance with model refinement.

References

Alzari, P. M., Berglund, H., Berrow, N. S., Blagova, E., Busso, D., Cambillau, C., Campanacci, V., Christodoulou, E., Eiler, S., Fogg, M. J., Folkers, G., Geerlof, A., Hart, D., Haouz, A., Herman, M. D., Macieira, S., Nordlund, P., Perrakis, A., Quevillon-Cheruel, S., Tarandeau, F., van Tilbeurgh, H., Unger, T., Luna-Vargas, M. P., Velarde, M., Willmanns, M. & Owens, R. J. (2006). Acta Crystallogr D Biol Crystallogr 62, 1103-1113.

Aslanidis, C. & de Jong, P. J. (1990). Nucleic Acids Res 18, 6069-6074.

Au, K., Berrow, N. S., Blagova, E., Boucher, I. W., Boyle, M. P., Brannigan, J. A., Carter, L. G., Dierks, T., Folkers, G., Grenha, R., Harlos, K., Kaptein, R., Kalliomaa, A. K., Levdikov, V. M., Meier, C., Milioti, N., Moroz, O., Muller, A., Owens, R. J., Rzechorzek, N., Sainsbury, S., Stuart, D. I., Walter, T. S., Waterman, D. G., Wilkinson, A. J., Wilson, K. S., Zaccai, N., Esnouf, R. M. & Fogg, M. J. (2006). Acta Crystallogr D Biol Crystallogr 62, 1267-1275.

Brzozowski, A. M. & Walton, J. (2001). Journal of Applied Crystallography 34, 97-101.

CCP4 (1994). Acta Crystallogr D Biol Crystallogr 50, 760-763.

DeLano, W. L. (2008). DeLano Scientific LLC.

Deutscher, M. P., Marshall, G. T. & Cudny, H. (1988). Proc Natl Acad Sci U S A 85, 4710-4714.

Emsley, P. & Cowtan, K. (2004). Acta Crystallogr D Biol Crystallogr 60, 2126-2132.

Fang, X. W., Yang, X. J., Littrell, K., Niranjanakumari, S., Thiyagarajan, P., Fierke, C. A., Sosnick, T. R. & Pan, T. (2001). Rna 7, 233-241.

Fogg, M. J. & Wilkinson, A. J. (2008). Biochem Soc Trans 36, 771-775.

Gouet, P., Courcelle, E., Stuart, D. I. & Metoz, F. (1999). Bioinformatics 15, 305-308.

Harlow, L. S., Kadziola, A., Jensen, K. F. & Larsen, S. (2004). Protein Sci 13, 668-677.

Ishii, R., Nureki, O. & Yokoyama, S. (2003). J Biol Chem 278, 32397-32404.

Kabsch, W. (1988). Journal of Applied Crystallography 21, 916-924.

Laskowski, R. A. (2001). Nucleic Acids Res 29, 221-222.

Mian, I. S. (1997). Nucleic Acids Res 25, 3187-3195.

Mildvan, A. S. (1997). Proteins 29, 401-416.

Murshudov, G. N., Vagin, A. A. & Dodson, E. J. (1997). Acta Crystallogr D Biol Crystallogr 53, 240-255.

Otwinowski, Z., Minor, W. & Charles W. Carter, Jr. (1997). Processing of X-ray diffraction data collected in oscillation mode, Vol. Volume 276, Methods in Enzymology, p. 307. Academic Press.

Pellegrini, O., Nezzar, J., Marchfelder, A., Putzer, H. & Condon, C. (2003). Embo J 22, 4534-4543.

Read, T. D., Peterson, S. N., Tourasse, N., Baillie, L. W., Paulsen, I. T., Nelson, K. E., Tettelin, H., Fouts, D. E., Eisen, J. A., Gill, S. R., Holtzapple, E. K., Okstad, O. A., Helgason, E., Rilstone, J., Wu, M., Kolonay, J. F., Beanan, M. J., Dodson, R. J., Brinkac, L. M., Gwinn, M., DeBoy, R. T., Madpu, R., Daugherty, S. C., Durkin, A. S., Haft, D. H., Nelson, W. C., Peterson, J. D., Pop, M., Khouri, H. M., Radune, D., Benton, J. L., Mahamoud, Y., Jiang, L., Hance, I. R., Weidman, J. F., Berry, K. J., Plaut, R. D., Wolf, A. M., Watkins, K. L., Nierman, W. C., Hazen, A., Cline, R., Redmond, C., Thwaite, J. E., White, O., Salzberg, S. L., Thomason, B., Friedlander, A. M., Koehler, T. M., Hanna, P. C., Kolsto, A.-B. & Fraser, C. M. (2003). Nature 423, 81.

Stams, T., Niranjanakumari, S., Fierke, C. A. & Christianson, D. W. (1998). Science 280, 752-755.

Studier, F. W. (2005). Protein Expr Purif 41, 207-234.

Symmons, M. F., Jones, G. H. & Luisi, B. F. (2000). Structure 8, 1215-1226.

Symmons, M. F., Williams, M. G., Luisi, B. F., Jones, G. H. & Carpousis, A. J. (2002). Trends Biochem Sci 27, 11-18.

Thompson, J. D., Higgins, D. G. & Gibson, T. J. (1994). Nucleic Acids Res 22, 4673-4680.

Vagin, A. & Teplyakov, A. (1997). Journal of Applied Crystallography 30, 1022-1025.

Wen, T., Oussenko, I. A., Pellegrini, O., Bechhofer, D. H. & Condon, C. (2005). Nucleic Acids Res 33, 3636-3643.

Zuo, Y. & Deutscher, M. P. (2001). Nucleic Acids Res 29, 1017-1026.